ORIGINAL PAPER

sciendo

Observation of intrapulse energy switching in standing-wave electron linac

Michał Matusiak [ID],
Tymoteusz Kosiński [ID],
Sławomir Wronka [ID],
Tomasz Zakrzewski [ID]

Abstract. For the development of an effective cargo-scanning system, an intrapulse energy switching has been tested at the National Centre for Nuclear Research (NCBJ) with the possibility to change the beam energy within a 4 μs pulse of the linear electron accelerator (linac). Modification of the electron energy is achieved through the beam-loading effect in a standing-wave accelerating structure equipped with a triode gun. Construction of the machine and the achieved results are presented in this article.

Keywords: Cargo scanning • Dual-energy imaging • X-ray imaging

M. Matusiak, T. Kosiński, S. Wronka✉, T. Zakrzewski
National Centre for Nuclear Research
Andrzeja Sołtana 7 Str., 05-400 Otwock-Świerk, Poland
E-mail: slawomir.wronka@ncbj.gov.pl

Introduction

The National Centre for Nuclear Research (NCBJ) has already achieved pulse-to-pulse energy switching in the Interlaced Energy Cargo Scanning System (CANIS) [1]. It allows us to obtain colored X-ray images of cargo, where different colors represent groups of identified materials: organic, nonorganic, and metal [2]. The unique construction of CANIS is based on the fast power switch, which is able to set the portion of high-power radiofrequency (RF) transmitted from the magnetron to an accelerating structure during each pulse and is fast enough to react within a short time between pulses.

Linear electron accelerators (linacs) typically work with a pulse repetition rate up to 300 Hz; it is limited by the magnetron average power equal to 0.1% of the peak power of the pulse. By shortening the pulse length, one can reach 500–1000 Hz in cargo linacs powered by 3.1 MW magnetrons. One of the methods to make the process of high-energy cargo scanning even faster is to switch the energy not between but during each pulse. When the detector line is properly designed and consists of fast scintillators with short afterglow, it can speed up the scanning process.

Such ideas have been presented already in previous research [3]. At the NCBJ, a demonstration of the intrapulse switching based on the beam-loading effect [4] was undertaken using a dedicated stand CANIS-2, equipped with a side-coupling, standing-wave accelerating structure [5]. Detailed studies covered dynamic energy measurements, repeatability, stability, and energy-switching effectiveness. We
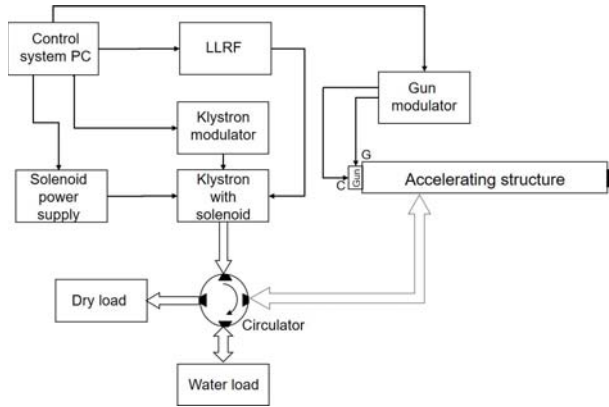
Fig. 1. Scheme of the CANIS-2 linac elements and connections. C – cathode–anode voltage; G – grid voltage; LLRF – low-level RF circuits for proper klystron pulse shaping.

focused especially on the 6–9 MeV energy range, preferred in train cargo scanners.

Intrapulse switching linac hardware

The general scheme of the CANIS-2 accelerator is presented in Fig. 1. To allow a wide beam-energy range, CANIS-2 consists of a 5 MW TH2157A klystron powered by ScandiNova K100 solid-state modulator. Accelerating structure with waveguide--coupling value equal to 1.9 is supplied via a four-port circulator. The solid-state modulator allows for the modification of the RF pulse time from 1 μs to 6 μs and the pulse repetition rate up to 300 Hz (depends on the peak power from klystron (PK) and pulse time so as not to exceed an average power of 7 kW).

Beam control is performed using the triode gun modulator, whereby a user can modify the cathode–anode voltage (C) within the range of 7–15 kV and the beam pulse time ranging from 1 μs to 6 μs. Beam-loading modification can be achieved dynamically by varying the grid voltage (G) level in the range from –150 V to 100 V, with a gun modulator switching time <500 ns. It corresponds to the gun current change from 0 A up to 1 A. All CANIS-2 elements are controlled by a personal computer (PC)-based control system. Other auxiliary systems such as a vacuum pump and a water-cooling system are not shown here but are also installed.

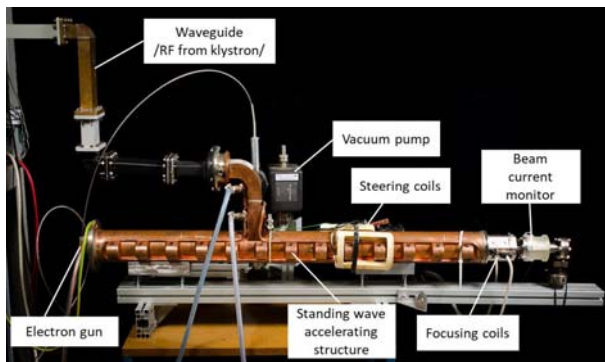The general view of the tested hardware is presented in Fig. 2.

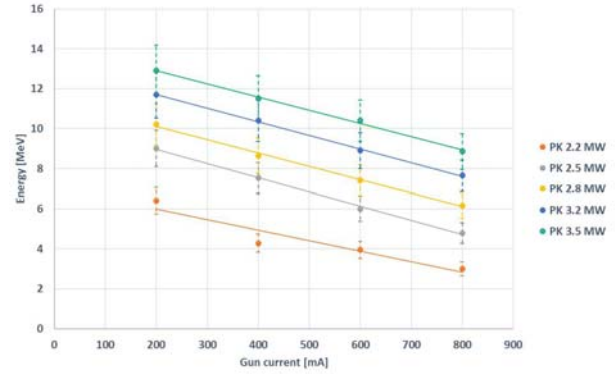**Fig. 2.** General view of CANIS-2 stand.

Fig. 3. Electron beam energy as a function of RF power from klystron (PK) and gun current. Linear fit is applied. The error bars represent the uncertainty of the magnetic spectrometer measurements.

Results of static measurement

At the beginning, no intrapulse switching was applied and we measured all the linac parameters and determined the proper working points. A map of the achieved beam energy values was created after a set of "static" measurements were performed with the following modified parameters: RF power level (the PK): 2.2–3.5 MW, electron beam current emitted from the gun: 200–800 mA. The value of the gun's high voltage was set at 12 kV and not modified, since it has a minor influence on the beam parameters.

The results for five different power settings are shown in Fig. 3. The linearity of the beam energy is clearly visible within the measurement error.

To efficiently switch the electrons' energy by beam loading in the 6–9 MeV range, a PK value equal to 2.8 MW was chosen. The electron beam energy was measured by a magnetic spectrometer capable of measuring the spectra up to 18 MeV. The results for selected working points at 2.8 MW RF power are presented in Fig. 4.

Observation of intrapulse switching

The magnetic spectrometer is a useful tool for static observations only, since every single measurement lasts 1–2 minutes. To observe the intrapulse energy
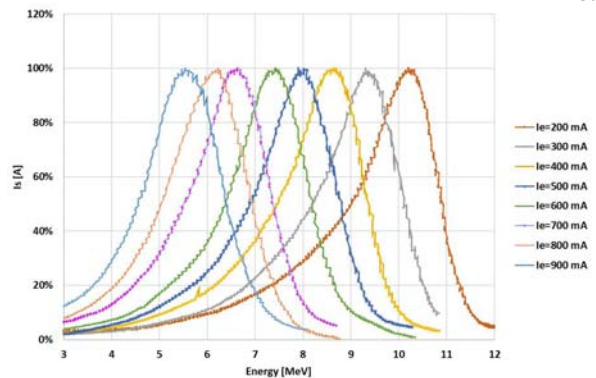

Fig. 4. Normalized electron beam energy spectra measured using a magnetic spectrometer for different beam currents (Ie). (Is – a current by magnetic spectrometer's Faraday cup).
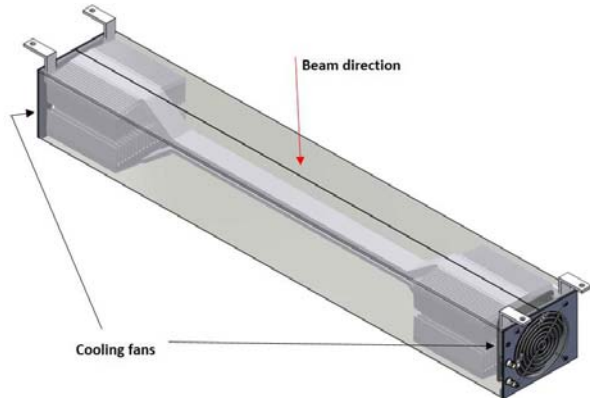
Fig. 5. Dedicated tool for dynamic electron beam energy measurements. The sensitive area is located in the middle, while both ends terminated in air-cooled radiators.

switching, a new, dedicated tool, able to handle dynamic visualization of the electron energy in time, had to be prepared. Therefore, a device for fast measurements, which consists of two electrically isolated aluminum plates, was designed (Fig. 5). Both plates were grounded via 50 Ω resistors and connected to a Rohde & Schwarz RTO2044 oscilloscope. The ratio of the charges deposited by the electron beam on the plates is directly related to the electron energy [6, 7].

The optimum thicknesses of the two aluminum end plates for the 6–9 MeV range were selected experimentally and were equal to 7.5 mm and 15 mm, respectively. For such thicknesses, both signals had clearly observable amplitudes. Before the measurements, the device was calibrated. For selected energies, the integrated charges collected in both aluminum plates (Q_1 and Q_2, respectively) during the accelerator pulse were measured, and the Q_1/Q_2 ratio was calculated. The relation between the beam energy and the Q_1/Q_2 ratio is shown in Fig. 6.

The best fit for the expression $E = f(Q_1/Q_2)$, showing the experimental relation of the integrals of the electron charge-deposition distributions in aluminum (presented in a previous paper [6]) has an exponential nature:

$$(1) \qquad E = a \times e^{\left(b \times \frac{Q_1}{Q_2}\right)}$$

where the values of the coefficients a and b are as follows: $a = 14.314$ MeV; $b = -0.639$.
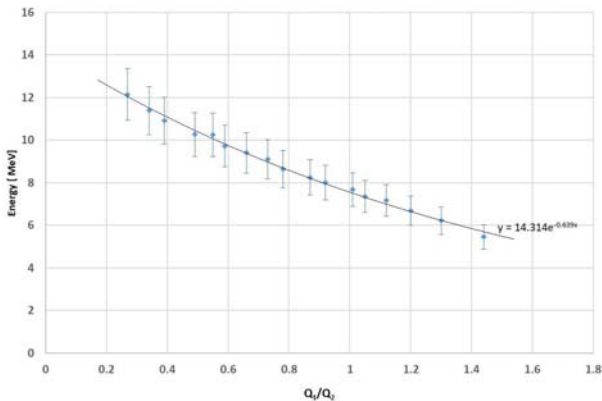

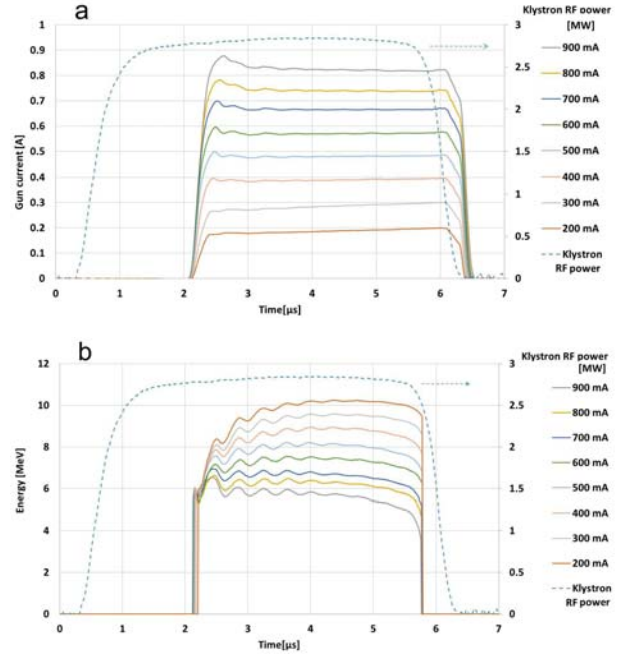**Fig. 6.** Calibration curve of the dual-plate device.

Fig. 7. Gun currents measured during the accelerator pulse, shown along with the RF pulse (a); electron energy at the accelerator exit in relation to time for different gun current settings, shown along with the RF pulse (b). All curves averaged over 1000 pulses.

Q_1 and Q_2, integrated charges collected in the two aluminum plates.

After the calibration procedure, the setup was ready for the dynamic experiments.

First, the beam energy was observed in relation to time during the accelerator pulse, for different beam currents and an RF power of 2.8 MW. The results are presented in Fig. 7.

As one can see, an electron beam was emitted with ~2 μs delay in relation to the klystron pulse, to ensure the correct filling of the standing-wave structure by the RF field. The gun modulator works in a stable way in a wide range of gun currents (Fig. 7a), although its effectiveness is lower for higher currents, i.e., when the measured values are below the settings. For higher electron beam energies, a longer time is required for nominal energy stabilization (Fig. 7b).

In the next step, intrapulse switching was tested by rapid modification of the beam current in the middle of the pulse, i.e., after ~2 μs. To switch between low and high energies, one should start with a high gun current and drop it down to lower values. An example of the control signals for switching realization is presented in Fig. 8. The red curve represents the beam current drop accomplished by the gun modulator ~1.5 μs after the switching trigger signal (SW trigger).

The effect of the energy switching is presented in Fig. 9. To set the correct beam energies, the exact values of the electron beam currents for both periods of the pulse time were tuned experimentally and 6 MeV is achieved at 720 mA, while 9 MeV is obtained at 270 mA.

In Fig. 9, both switching directions are shown, i.e., 6 MeV → 9 MeV and 9 MeV → 6 MeV. For final application, i.e., cargo scanning, the first case is more
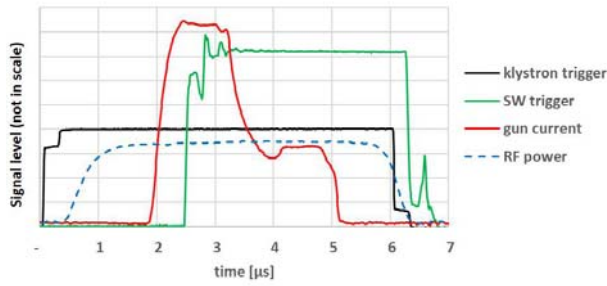
Fig. 8. Oscillogram of the control signals for intrapulse switching.
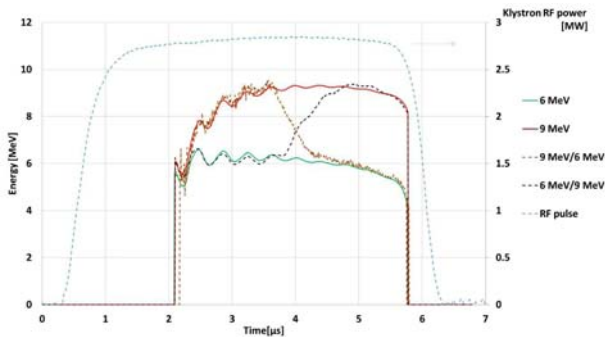

Fig. 9. Intrapulse energy switching.

useful. As one can see, building up of the nominal energy value at 9 MeV first takes more time, which causes blurring of the energy spectrum. Therefore, for further studies, the 6 MeV → 9 MeV case was preferred, and for this scenario, the histogram based on the black curve in Fig. 9 was prepared and is shown in Fig. 10.

Two clear peaks at 6 MeV and 9 MeV confirm that the method works properly. However, the cargo scanning process can be further improved when fast scintillating crystals without long afterglow are used (e.g., $(Lu,Y)_2SiO_5$:Ce [LYSO] [8]). Detector triggers should then select only the pulse regions marked in Fig. 11b. In effect, the peaks in the electron energy histogram are well separated (Fig. 11a) in comparison to Fig. 10, which allows for better material discrimination.

Finally, as a cross-check, the "static" measurement with the magnetic spectrometer was repeated but with the intrapulse energy switching activated.

The obtained result, presented in Fig. 12, agrees well with what one may expect. Two peaks are clearly visible and located in correct places. The different amplitudes of the peaks are related to the unequal
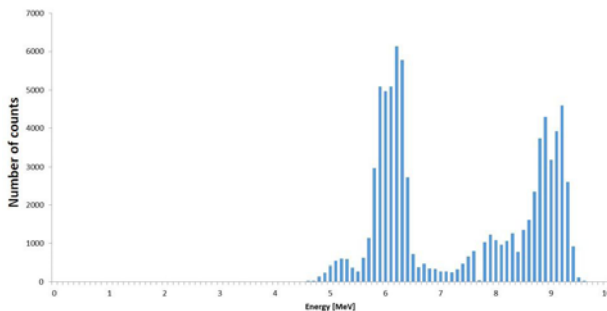

Fig. 10. Histogram of electron beam energy obtained during the 6 MeV → 9 MeV energy switching.
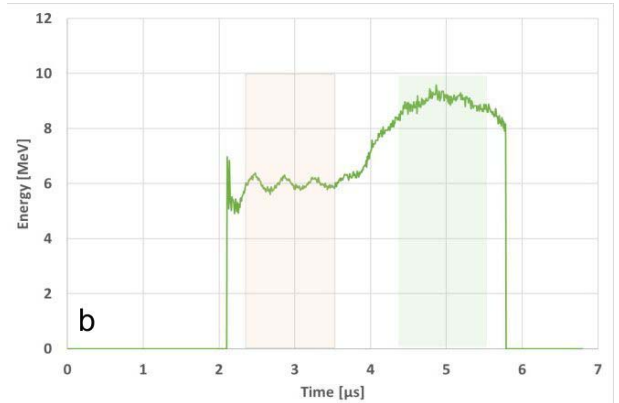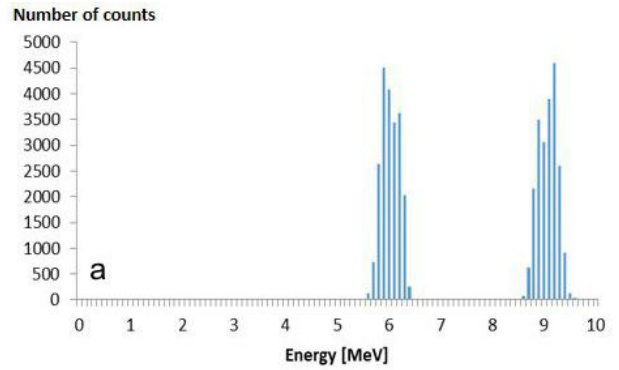

Fig. 11. Energy histogram (a) obtained in selected parts of the electron beam pulse (b).
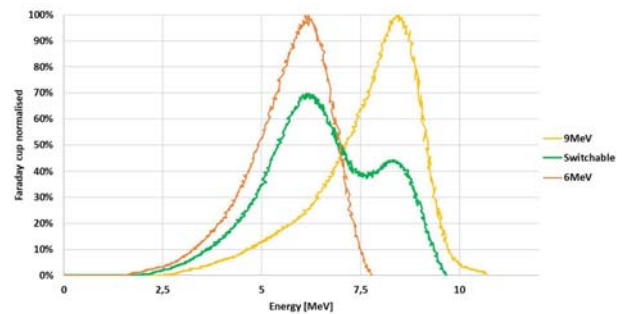

Fig. 12. Energy spectrum measured by the magnetic spectrometer, shown along with the spectra measured without switching.

time lengths of the pulses, while the static measurements are normalized.

Conclusions

The main goal, i.e., observation of intrapulse switching, has been achieved on a dedicated CANIS-2 experimental stand built at the NCBJ. The measurements were focused particularly on the energy range useful for train-scanning applications, i.e., 6–9 MeV. Optimum values were found when the electron standing-wave accelerating structure was powered by a klystron at 2.8 MW. Owing to the rapid modification of the electron gun current from 720 mA to 270 mA, the beam-loading effect results in the electron energy change from 6 MeV to 9 MeV during each linac pulse. For the dynamic energy measurements, the well-known multiplate method

was used. Two well-separated energy peaks can be seen in the measured energy histogram.

The imaging detector line of the cargo-scanning system using intrapulse switching linac should consist of fast scintillating crystals and should be triggered selectively, to further improve the quality of the reconstructed images.

The klystron used in the CANIS-2 stand can be easily replaced in final applications by the commonly used 3.1 MW magnetron. Moreover, another energy range, i.e., 4/6 MeV, popular for truck scanning, can be achieved at a lower RF power with the same method.

ORCID

T. Kosiński http://orcid.org/0000-0003-2052-4269
M. Matusiak http://orcid.org/0000-0002-8239-6971
S. Wronka http://orcid.org/0000-0003-3277-138X
T. Zakrzewski http://orcid.org/0000-0002-9210-9972

References

1. Wronka, S. (2016). *Interlaced energy linac with smooth energy regulation*. Warsaw: Institute of Electronics Systems, Warsaw University of Technology.

2. Ogorodnikov, S., & Petrunin, V. (2002). Processing of interlaced images in 4–10 MeV dual energy customs system for material recognition. *Phys. Rev. ST Accel. Beams*, *5*, 104701. https://doi.org/10.1103/PhysRevSTAB.5.104701.

3. Saverskiy, A. Y., Dinca, D. C., & Rommel, J. M. (2014). Cargo and container X-ray inspection with intra-pulse multi-energy method for material discrimination. In 23rd Conference on Application of Accelerators in Research and Industry, CAARI 2014.

4. Arai, S., Katayama, T., Tojyo, E., & Yoshida, K. (1980). Beam-loading effects in a standing-wave accelerator structure. *Part. Accel.*, *11*, 103–111.

5. Matusiak, M., & Wronka, S. (2016). PL Patent No. 231603. Warsaw: The Patent Office of the Republic of Poland.

6. Fuochi, P. G., Lavalle, M., Martelli, A., Corda, U., Kovacs, A., Hargittai, P., & Mehta, K. (2005). Energy device for monitoring 4–10 MeV industrial electron accelerators. *Nucl. Instrum. Methods Phys. Res. Sect. A-Accel. Spectrom. Dect. Assoc. Equ.*, *546*(3), 385–390.

7. Fuochi, P. G., Lavalle, M., Martelli, A., Corda, U., Kovacs, A., Hargittai, P., & Mehta, K. (2003). Electron energy device for process control. *Radiat. Phys. Chem.*, *67*, 593–598.

8. Valais, I. G., Michail, C. M., David, S. L., Konstantidinis, A., Cavouras, D. A., Kandarakis, I. S., & Panayiotakis, G. S. (2008). Luminescence emission properties of $(Lu,Y)_2SiO_5$:Ce (LYSO:Ce) and $(Lu,Y)AlO_3$:Ce single crystal scintillators under medical imaging conditions. *IEEE Trans. Nucl. Sci.*, *55*(2), 785–789.